Nonlin. Processes Geophys. Discuss., 2, 1447–1479, 2015
www.nonlin-processes-geophys-discuss.net/2/1447/2015/
doi:10.5194/npgd-2-1447-2015

Nonlinear Processes in Geophysics Discussions
Open Access

Wavelet analysis of the singular spectral reconstructed time series to study the imprints of Solar–ENSO–Geomagnetic activity on Indian climate

S. Sri Lakshmi[1] and R. K. Tiwari[2]

[1]University Centre for Earth and Space Sciences, University of Hyderabad, 500 046 Hyderabad, India
[2]National Geophysical Research Institute, Uppal Road, 500 007 Hyderabad, India

Received: 24 February 2015 – Accepted: 2 September 2015 – Published: 28 September 2015

Correspondence to: S. Sri Lakshmi (srilakshmi.ucess@gmail.com)

Published by Copernicus Publications on behalf of the European Geosciences Union & the American Geophysical Union.

Abstract

In order to study the imprints of solar–ENSO–geomagnetic activity on the Indian Subcontinent, we have applied the Singular Spectral Analysis (SSA) and wavelet analysis to the tree ring temperature variability record from the western Himalayas. The data used in the present study are the Solar Sunspot Number (SSN), Geomagnetic Indices (aa Index), Southern Oscillation Index (SOI) and tree ring temperature record from western Himalayas (WH), for the period of 1876–2000. The SSA and wavelet spectra reveal the presence of 5 years short term ENSO variations to 11 year solar cycle indicating the influence of both the solar–geomagnetic and ENSO imprints in the tree ring data. The presence of 33-year cycle periodicity suggests the Sun-temperature variability probably involving the induced changes in the basic state of the atmosphere. Our wavelet analysis for the SSA reconstructed time series agrees with our previous results and also enhance the amplitude of the signals by removing the noise and showing a strong influence of solar–geomagnetic and ENSO patterns throughout the record. The solar flares are considered to be responsible for cause in the circulation patterns in the atmosphere. The net effect of solar–geomagnetic processes on temperature record thus appears to be the result of counteracting influences on shorter (about 5–6 years) and longer (about 11–12 years) time scales. The present analysis thus suggests that the influence of solar processes on Indian temperature variability operates in part indirectly through ENSO, but on more than one time scale. The analyses hence provides credible evidence for teleconnections of tropical pacific climatic variability with Indian climate ranging from interannual-decadal time scales and also demonstrate the possible role of exogenic triggering in reorganizing the global earth–ocean–atmospheric systems.

Discussion Paper | Discussion Paper | Discussion Paper | Discussion Paper |

NPGD

2, 1447–1479, 2015

Study of the imprints of Solar–ENSO–Geomagnetic activity on Indian climate

S. Sri Lakshmi and R. K. Tiwari

1 Introduction

Several recent studies of solar–geomagnetic effects on climate have been examined on both global as well as on regional scales (Lean and Rind, 2008; Benestaed and Schmidt, 2009; Meehl, 2009; Kiladis and Diaz, 1989; Pant and Rupa Kumar, 1997; Gray et al., 1992; Wiles et al., 1998; Friis and Svensmark, 1997; Rigozo et al., 2005; Feng et al., 2003; Tiwari and Sri Lakshmi, 2009; Chowdary et al., 2006, 2014; Appenzeller et al., 1998; Proctor et al., 2002; Tsonis et al., 2005; Freitas and Mclean, 2013). The Sun's long-term magnetic variability is the primary driver of climatic changes. The magnetic variability (mostly short-term components) is due to the disturbances in Earth's magnetic fields caused by the solar activity, which is usually indicated by indices of geomagnetic activity. The Sun's magnetic variability modulates the magnetic and particulate fluxes in the heliosphere. This determines the interplanetary conditions and imposes significant electromagnetic forces and effects upon planetary atmospheres. All these effects are due to the changing solar-magnetic fields which are relevant for planetary climates, including the climate of the Earth. The Sun–Earth relationship varies on different time scales of days to years bringing a drastic influence on the climatic patterns. The ultimate cause of solar variability, at time scales from decadal to centennial to millennial or even longer scales, has its origin in the solar dynamo mechanism. During the solar maxima, huge amounts of solar energy particles are released, thereby causing the geomagnetic disturbances. The 11 years solar cycle acts an important driving force for variations in the space weather, ultimately giving rise to climatic changes. Therefore, it is very important to understand the origin of space climate by analyzing the different proxies of solar magnetic variability. The another most important climate variation is El Niño–Southern Oscillation (ENSO) events, which impact the global oceanic and atmospheric circulations which thereby produce droughts, floods and intense rainfall in certain regions. The strong coupling and interactions between the Tropical Ocean and atmosphere play a major role in the development of global climatic system. The El Niño events generally recur approximately every 3–5 years with

NPGD
2, 1447–1479, 2015

large events spaced around 3–7 years apart. The El Niño–Southern Oscillation (ENSO) phenomena has shown huge impact on the Asian monsoon (Cole et al., 1993), Indian monsoon (Chowdary et al., 2006, 2014) as well as globally (Horel and Wallance, 1981; Barnett, 1989; Yasunari, 1985; Nicholson, 1997). In particular, the El Niño, solar, geomagnetic activities are the major affecting forces on the decadal and interdecadal temperature variability on global and regional scales in a direct/indirect way. Recent studies (Frohlich and Lean, 2004; Steinhilber et al., 2009) indicate the possible influence of solar activity on Earth's temperature/climate on multidecadal time scales. The 11 year solar cyclic variations observed from the several temperature climate records also suggest the impact of solar irradiance variability on terrestrial temperature (Budyko, 1969; Friis and Lassen, 1991; Friis and Svensmark, 1997; Kasatkina et al., 2007). The bidecadal (22 years) called the Hale cycle, is related to the reversal of the solar magnetic field direction (Lean et al., 1995; Kasatkina et al., 2007). The 33 year cycle (Bruckener cycle) is also caused by a solar origin, but it is a very rare cycle (Kasatkina et al., 2007). The 2–7 years ENSO cyclic pattern and its possible coupling process is the major driving force for the temperature variability (Gray et al., 1992; Wiles et al., 1998; Mokhov et al., 2000; Rigozo et al., 2007; Kothawale et al., 2010). El-Borie et al., 2010 have indicated the possible contributions for both the solar and geomagnetic activities components (aa). Studies (El-Borie and Al-Thoyaib, 2006; El-Borie et al., 2007) have indicated that the global temperature should lag the geomagnetic activity, with a correlation that reaches a maximum when the temperature lags by 6 years. Mendoza et al. (1991) reported on possible connections between solar activity and El Niño's, while Reid and Gage (1988) and Reid (1991) reported on the similarities between the 11-year running means of monthly sunspot numbers and global sea surface temperature. These findings suggest that there is possible strong coupling between temperature–ENSO and solar–geomagnetic signals. The mean global temperature of the Earth's surface also plays a very important role in bringing climatic changes. Studies are being made to understand the detailed climatic changes of India in the past millennium using various proxy records e.g. ice cores, lake sediments, glacier fluctuations, peat deposits

NPGD
2, 1447–1479, 2015

S. Sri Lakshmi and R. K. Tiwari

etc. The availability of high-precision and high-resolution palaeoclimatic information for longer time scale from the Indian subcontinent is very less. In recent years, tree-ring data is promising proxy to retrieve high resolution past climatic changes from several geographical regions of India (Bhattacharyya et al., 1988, 1992, 2006; Hughes, 1992; Bhattacharyya and Yadav, 1996; Borgaonkar et al., 1996; Chaudhary et al., 1999; Yadav et al., 1999; Bhattacharyya and Chaudhary, 2003; Shah et al., 2007). It has been recorded that tree-ring based climatic reconstructions in India generally do not exceed beyond 400 years records except at some sites in the northwest Himalaya. Thus, a long record of tree-ring data is needed to extend available climate reconstruction further back to determine climatic variability in sub-decadal, decadal and century scale. However, non availability of older living trees in most of the sites is hindering the preparation of long tree chronology. In previous study (Tiwari and Srilakshmi, 2009) have studied the periodicities and non-stationary modes in the tree ring temperature data from the same region (AD 1200–2000). To gain significant connections among the solar–geomagnetic–ENSO “triad” phenomena on tree ring width in detail for the time period from 1876–2000, we have applied here the Singular spectral analysis (SSA) and the wavelet spectral analysis for Sunspot data, Geomagnetic data (aa Index), Troup Southern Oscillation Index (SOI) and the western Himalayas tree ring data. Our main objective here is to present a wavelet-based analysis of SSA reconstructed time series to focus on the evidence for the ENSO–solar–geomagnetic connections in comparison to ENSO–geomagnetic and solar–ENSO connections.

2 Source and nature of data

The set of data analyzed in our work includes the time series of (1) smoothed sunspot number for solar activity, (2) geomagnetic activity data (aa indices), (3) troup Southern Oscillation Index (SOI) for the study of El Niño–Southern Oscillation called ENSO, (4) western Himalayan temperature variability record. All these four data sets are analyzed for a common period of 125 years spanning over 1876–2000.

The monthly sunspot number data is obtained from the Sunspot Index Data Center http://astro.oma.be/SIDC/. The Troup SOI data is obtained from the Bureau of Meteorology of Australia, http://www.bom.gov.au/climate/. The data for geomagnetic activity, aa Index, was provided by the National Geophysical Data Center, NGDC, (http://www.ngdc.noaa.gov/stp/GEOMAG/aastar.html). The aa Index is a measure of disturbances level of Earth's magnetic field based on magnetometer observations at two, nearly antipodal, stations in Australia and England. In recent studies, the tree ring proxy climate indicators have been potentially used for extracting information regarding past seasonal temperature or precipitation/drought based on the measurements of annual ring width. The detailed description of the data has been presented elsewhere (Yadav et al., 2004). A brief account of the data pertinent to the present analysis, however, is summarized here. The tree ring data being analyzed here is one of the best temperature variability records (1876 to 2000) of the pre-monsoon season in the western Himalayas. The mean temperature series is obtained from nine weather stations including both from high and low elevation areas in the western Himalayas. Temperature variability history is based on widely spread pure Himalayan cedar (*Cedrus deodara* (Roxb.) G. Don) trees and characterizes all the sites with almost no ground vegetation and thereby minimizes individual variation in tree-ring sequences induced by inter tree competition (Yadav et al., 2004). The mean chorological structure is based on in total 60 radii from 45 trees, statistical feature of which show that the chronology is suitable for dendro-climatic studies back to AD 1226 (Yadav et al., 2004).

3 Methods applied

To analyze the temporal series and to find the climatic structure, we have here applied three methods: Principal component analysis (PCA), Singular Spectral analysis (SSA) and wavelet analysis.

NPGD
2, 1447–1479, 2015

3.1 Principal component analysis (PCA)

As a preliminary analysis, we have applied the Principle Component Analysis (PCA) to the data sets to extract the principle components. PCA technique is applied for the reduction and extraction for dimensionality of the data and to rate the amount of variation present in the original data set. The purpose to apply the PCA is to identify patterns in the given time series. The new components thereby obtained by the PCA analysis are termed as PC1, PC2, PC3 and so on, (for the first, second and third principal components) are independent and decrease the amount of variance from the original data set. PC1 (the first component) captures most of the variance; PC2 captures the second most of the variance and so on. These components are treated as climatic factors or climatic structures.

3.2 Singular spectral analysis

The Singular Spectrum Analysis (SSA) method was developed as the new time series method since 1970s. This method is designed to extract as much information as possible from a short, noisy time series without any prior knowledge about the dynamics underlying the series (Broomhead and King, 1986; Vautard and Ghil, 1989). The method is a form of principal component analysis (PCA) applied to lag-corrections structures of the time series. The basic SSA decomposes an original time series into a new series which consists of trend, periodic or quasi-periodic and white noises according to the singular value decomposition (SVD) and provides the reconstructed components (RCs). The basic steps involved in SSA are: decomposition (involves embedding, singular value decomposition – SVD) and reconstruction (involves grouping, and diagonal averaging). Embedding decomposes the original time series into the trajectory matrix; SVD turns the trajectory matrix into the decomposed trajectory matrices. The reconstruction stage involves grouping to make subgroups of the decomposed trajectory matrices and diagonal averaging to reconstruct the new time series from the subgroups.

NPGD
2, 1447–1479, 2015

Step1: decomposition

a. Embedding: the first step in the basic SSA algorithm is the embedding step where the initial time series change into the trajectory matrix. Let the time series be $Y = \{y_1, \ldots, y_N\}$ of length N without any missing values. Here the window length L is chosen such that $2 < L < N/2$ to embed the initial time series. We map the time series Y into the L lagged vectors, $\boldsymbol{Y}_i = \{y_i, \ldots, y_{i+L-1}\}$ for $i = 1 \ldots K$, where $K = N - L + 1$. The trajectory matrix $\mathbf{T}_Y$ ($L \times K$ dimensions) is written as:

$$\mathbf{T}_Y = \begin{pmatrix} \boldsymbol{Y}_1 \\ \boldsymbol{Y}_2 \\ \vdots \\ \boldsymbol{Y}_K \end{pmatrix}. \tag{1}$$

b. Singular Value Decomposition (SVD): here we apply SVD to the trajectory matrix $\mathbf{T}_Y$ to decompose and obtain $\mathbf{T}_Y = \mathrm{UDV}'$ called eigentriples; where $\mathbf{U}_i$ ($K \times L$ dimensions; $1 < i < L$) is an orthonormal matrix; $\mathbf{D}_i$ ($1 < i < L$) is a diagonal matrix of order L; $\mathbf{V}_i$ ($L \times L$ dimensions; $1 < i < L$) is a square orthonormal matrix.

The trajectory matrix is thus written as

$$\mathbf{T}_Y = \sum_{i=1}^{d} \mathbf{U}_i \sqrt{\lambda_i} \mathbf{V}_i^T; \tag{2}$$

where the ith eigen triple of $\mathbf{T}_i = \mathbf{U}_i \cdot \sqrt{\lambda_i} \cdot \mathbf{V}_i^T$, $I = 1, 2, 3 \ldots, d$ in which $d = \max(i : \sqrt{\lambda_i} > 0)$.

Step1: reconstruction

c. Grouping: here the matrix $\mathbf{T}_i$ is decomposed into subgroups according to the trend, periodic or quasi-periodic components and white noises. The grouping step

NPGD

2, 1447–1479, 2015

of the reconstruction stage corresponds to the splitting of the elementrary matrices $\mathbf{T}_i$ into several groups and summing the matrices within each group. Let $I = \{i_1, i_2, \ldots, i_p\}$ be the group of indices $i_1, \ldots i_p$. Then the matrix $\mathbf{T}_I$ corresponding to the group I is defines as $\mathbf{T}_I = T_{i1} + T_{i2} + \ldots T_{ip}$. The split of the set of indices $J = 1, 2, \ldots, d$ into the disjoint subsets $I_1, I_2, \ldots I_m$ corresponds to

$$T = T_{I1} + T_{I2} + \ldots T_{Im}. \tag{3}$$

The sets $I_1, \ldots, I_m$ are called the eigen triple grouping.

d. Diagonal averaging: the diagonal averaging transfers each matrix $\mathbf{T}$ into a time series, which ia an additive component of the intital times series $\boldsymbol{Y}$. if z_{ij} strands for a element matrix $\mathbf{Z}$, the kth term of the resulting series is obtained by averaging z_{ij} over all I, j such that $i + j = k + 2$. This is called diagonal averaging or the Hankelization of the matrix $\mathbf{Z}$. The Hankel matrix $\mathbf{HZ}$, is the trajectory matrix corresponding to the series obtained by the result of diagonal averaging.

Considering Eq. (3), let $\mathbf{X}$ $(L \times K)$ matrix with elements x_{ij}, where $1 \le i \le L$, $1 \le j \le K$. Here diagonal averaging transforms matrix $\mathbf{X}$ to a series $g_0, \ldots, g_{T-1}$ using the formula:

$$g_k = \begin{cases} \frac{1}{k+1} \sum_{m=1}^{k+1} x^*_{m,k-m+2} & 0 \le k < L^* - 1 \\ \frac{1}{L^*} \sum_{m=1}^{L^*} x^*_{m,k-m+2} & L^* - 1 \le k < K^* \, . \\ \frac{1}{T-k} \sum_{m=k-k^*+2}^{N-k+1} x^*_{m,k-m+2} & K^* - 1 \le k < T \end{cases} \tag{4}$$

This diagonal averaging by Eq. (4) applied to the resultant matrix $\mathbf{X}_{In}$, produces time series $\boldsymbol{Y}_n$ of length T. For such signal characteristics, it is essential to examine the time-frequency pattern as to understand whether a particular frequency is temporally consistent or inconsistent. Hence for non-stationary signals, we need a transform that will be useful to obtain the frequency content of the time series/signal as a function of time. An alternative method for studying the non-stationarity of the time series is wavelet transform. For non-stationary signals, wavelets decomposition would be the most appropriate because the analyzing functions (the wavelets function) are localized both in time and frequency.

3.3 Wavelet spectral analysis

During the past decades, wavelet analysis has become a popular method for the analysis of aperiodic and quasi-periodic data (Grinsted et al., 2004; Jevrejeva et al., 2003; Torrence and Compo, 1998; Torrence and Webster, 1999). It has become an important tool for studying localized variations of power within a time series. By decomposing a time series into time-frequency space, the dominant modes of variability and their variation with respect to time can be identified. The wavelet transform has various applications in geophysics, including tropical convection (Weng and Lau, 1994), the El Niño–Southern Oscillation (Gu and Philander, 1995), etc. We have performed wavelet analysis to locate the specific events found in the datasets. The results give us more insight information about these variables in frequency-time mode.

A wavelet transform requires the choice of analyzing function or "mother wavelet" that have the specific property of time-frequency localization. They are functions generated from one single function Ψ, which is called mother wavelet, by dilations and translations. The continuous wavelet transform revolves around decomposing given time series into scale components for identifying oscillations occurring at fast (time) scale and other at slow scales. Mathematically, the continuous wavelets transform of a time series $f(t)$ can be given as:

$$W_{\psi}(f)(a,b) = \frac{1}{\sqrt{a}} \int_{-\infty}^{\infty} f(t)\psi\left(\frac{t-b}{a}\right)\mathrm{d}t. \tag{5}$$

Here $f(t)$ represents time series, Ψ is the base wavelets function (in the present case, Morlet function), with length that is much shorter than the time series $f(t)$. W stands for wavelet coefficients. The variable "a" is scale factor that determines the frequency (or scale) so that varying "a" gives rise to spectrum. The factor "b" is related to the shift of the analysis window in time so that varying b represents the sliding method of the wavelet over $f(t)$.

In several recent analyses, complex morlet wavelet has been found useful for geophysical time series analysis. The morlet is mostly used to find out areas where there is high amplitude at certain frequencies. The complex Morlet wavelet can be represented by a periodic sinusoidal function with a Gaussian envelope and is excellent for Morlet wavelet may be defined mathematically, as follows:

$$\psi(t) = \pi^{-1/4} e^{-i\omega_0 t} e^{-t^2/2} \tag{6}$$

where ω_0 is a non-dimensional value. ω_0 is chosen to be 5 to make the highest and lowest values of ψ approximately equal to 0.5, thus making the admissibility condition satisfied. The complex valued morlet transform enables to extract information about the amplitude and phase of the signal to be analyzed. Wavelet transform preserves the self-similarity scaling property, which is the inherent characteristic feature of deterministic chaos. The continuous wavelet transform has edge artifacts because the wavelet is completely localized in time. The cone of influence (COI) is the area in which the wavelet power caused by a discontinuity at the edge has dropped to e^{-2} of the value to the edge. The statistical significance of the wavelet power can be assessed relative to the null hypotheses that the signal is generated by a stationary process with a given background power spectrum (P_k) of first order autoregressive (AR1) process (Grinsted et al., 2004).

$$P_k = \frac{1-\alpha^2}{|1-\alpha e^{-2i\pi k}|^2} \tag{7}$$

where k is Fourier frequency index.

NPGD
2, 1447–1479, 2015

The cross wavelet transform is applied to two time series to identify the similar patterns which are difficult to assess from a continuous wavelet map. Cross wavelet power reveals areas with high common power. The cross wavelet of two time series $x(t)$ and $y(t)$ is defined as $W^{XY} = W^x W^{y^*}$, where * denotes complex conjugate. The cross wavelet power of two time series with background power spectra P_k^X and P_k^Y is given as

$$D\left(\frac{|W_n^X(s)W_n^{Y*}(s)|}{\sigma X \sigma Y} < p\right) = \frac{Z_\nu(p)}{\nu}\sqrt{P_k^X P_k^Y}, \tag{8}$$

where $Z_\nu(p)$ is the confidence level associated with the probability p for a pdf defined by the square root of the product of the two χ^2 distributions (Torrence and Compo, 1998). The cross wavelet analysis gives the correlation between the two time series as function of period of the signal and its time evolution with a 95 % confidence level contour. The statistical significance is estimated using red noise model.

Wavelet coherence is another important measure to assess how coherent the cross wavelet spectrum transform is in time frequency space. The wavelet coherence of two time series is defined as (Torrence and Webster, 1998)

$$R_n^2(s) = \frac{\left|S\left(s^{-1}W_n^{XY}(s)\right)\right|^2}{S\left(s^{-1}\left|W_n^X(s)\right|^2\right)\cdot S\left(s^{-1}\left|W_n^Y(s)\right|^2\right)} \tag{9}$$

where S is a smoothing operator. The smoothing operator is written as $S(W) = S_{\text{scale}}(S_{\text{time}}(W_n(s)))$, where S_{scale} denotes smoothing along the wavelet scale axis and S_{time} smoothing in time. Here for the morelet wavelet, the smoothing operator is

NPGD
2, 1447–1479, 2015

$$S_{\text{time}}(W)|_s = \left(W_n(s) \cdot c_1^{\frac{-t^2}{2s^2}} \right) \quad (10)$$

$$S_{\text{time}}(W)|_s = (W_n(s) \cdot c_2 \Pi(0.6s))_n| \quad (11)$$

where c_1 and c_2 are normalization constants and Π is the rectangle function. The factor of 0.6 is empirically determined scale decorrelation length of the Morelet wavelet (Torrence and Compo, 1998). The statistical significance level of the wavelet coherence is estimated using the Monte Carlo methods (Grinsted et al., 2004).

4 Results and discussion

In the present study, we have taken the data sets from the period of 1876–2000 and analyzed using the PCA, SSA and wavelet spectral analysis. Figure 1 shows the four time series: (1) smoothed sunspot number for solar activity; (2) geomagnetic (aa indices); (3) troup Southern Oscillation Index (SOI) for the study of El Niño–Southern Oscillation called ENSO and (4) western Himalayan temperature variability record that are analyzed in the present work. It is evident from Fig. 1 that both WH record and the SOI data appear irregular and random, while sunspot numbers have a clear cyclic character. The visual inspection of the western Himalayas tree ring record exhibits distinct temperature variability at a number of different time scales. This variability might be suggestive of coupled global ocean–atmospheric dynamics or some other factors, such as deforestation, anthropogenic, high latitudinal influence etc. (Yadav et al., 2004).

But however it is quite difficult to differentiate such a complex climate signals visually and difficult to infer any clear oscillation without the help of powerful mathematical methods. Hence, for the identification of any oscillatory components and understanding the climatic variations on regional and global scale, we have applied the PCA, SSA and wavelet analysis. As a preliminary step we have applied the PCA and calculated the principal components (PCs) for the first four eigen triples (PC1, PC2, PC3,

NPGD
2, 1447–1479, 2015

PC4) for the given data sets (Fig. 2). Figure 3 shows the power spectra of the principal components (PCs) for the four data sets shown in Fig. 2. From this figure, it is observed power spectra of PC1–4 for the sunspot data exhibits high power at 124, 11, 4–2.8 years. The presence of high solar signal at 124 years indicates the quasi-stable oscillatory components in the data. The power spectra of geomagnetic data also shows the presence of strong signals at 124, 10–11, 4–2 years suggesting a strong link of solar–geomagnetic activity. The power spectra of WH temperature data shows strong high power at ~ 62 years, 32–35, 11, 5 years and 2–3 years suggesting a strong influence of solar–geomagnetic–ENSO effects on the Indian climate system. A dominant amplitude is found at 32–35 years corresponding to AMO cycles These results can be better confirmed by applying the mathematical tools of SSA and wavelet analysis.

To explore the stationary characteristics of these peaks obtained by the PCA, we have applied the morlet based wavelet transform approach (Holschneider, 1995; Foufoula-Georgiou and Kumar, 1995; Torrence and Compo, 1998; Grinsted et al., 2004). The wavelet spectrum identifies the main periodicities in the time series and helps to analyze the periodicties with respect to time. Figure 4 shows the wavelet spectrum for the (a) smoothed sunspot number for solar activity (SSN) (b) western Himalayan (WH) temperature variability record (c) geomagnetic activity and (d) troup Southern Oscillation Index (SOI). From the wavelet spectrum of sunspot time series (Fig. 4a), the signal near 11-year is the strongest feature and is persistant during the entire series indicating the non-stationary behavior of the sunspot time series. The wavelet spectrum of SOI (Fig. 4c) shows strong amplitudes in the interval of 2–8 years. The signal is non-stationary with the periodicities alternating ie. present at sometimes and absent in others. The wavelet power spectrum of the western Himalayan temperature variability (Fig. 4b) reveals significant power concentration at interannual time scales of 3–5 years and at 11 years solar time scales. A dominant amplitude modes is also seen in the low frequency range at around 35–40 years (at periods 1930–1980) corresponding to AMO cycles. Our result agrees well with the results of other climate reconstructions (Mann et al., 1995) from tree rings and other proxies. The observed variability in AMO periodicity has also been reported in other tree ring record (Gray et al., 2004). The statistical significance of the wavelet power spectrum is tested by a Monte Carlo method (Torrence and Compo, 1998). The WH spectra depicting statistically significant powers at around 5, 11 and 33 years above the 95 % significance level, suggests a clear picture of the imprint of sunspot–geomagnetic and ENSO on the tree ring data. The wavelet power spectrum of the geomagnetic record (Fig. 4d) indicates significant power on shorter scales around 2, 4–8, 11 years period.

In order to have the better visualization of similar periods in two time series and for the interpretation of the results, cross wavelet spectrum has been applied. Figure 5 shows the cross wavelet spectrum of the (a) SSN–WH temperature data (b) WH data–SOI and (c) SSN–SOI data. The contours (dark black lines) are the enclosing regions where wavelet cross power is significantly higher, at 95 % confidence levels. The wavelet cross-spectra of WH–SSN (Fig. 5a) show statistically significant high power over a period of 1895–1985 in 8–16 years band. It is seen that the WH–SOI cross-spectra (Fig. 5b), the high power is observed at 2–4 year band and 8–16 years as well. The SSN–SOI spectra (Fig. 5c) shows a strong correlation at 11 years solar cycle stronger during 1910–1950 and 1960–2000 (Rigozo et al., 2002, 2003) suggesting the strongest El Niño and La Nina events indicating solar modulation on ENSO. These results show a good correspondence in response of growth of the tree ring time series during the intense solar activity. Hence the results strongly support the possible origin of these periodicities from Solar and ENSO events. The interesting conclusion from Fig. 5 is that WH–sunspot connections are strong at 11 years, ENSO–sunspot also exhibit strong power around 11 years; the WH–ENSO connections are spread over three bands, the 2–4, 4–8 and 8–16 years, covering the solar cycle and its harmonics; the WH–geomagnetic exhibits strong connections around 2–4, 4–6, 11 and 35–40 years indicating the influence of solar–geomagnetic activity on Indian climate.

The Singular spectral analysis (SSA) is performed for all the four data sets with window length of 40. The SSA spectra with 40 singular values and its corresponding reconstructed series (varying from RC1–15 in some cases) are plotted are shown in

NPGD
2, 1447–1479, 2015

Fig. 6. The important insight of SSA spectra is checking the breaks in the eigen value spectra. As a rule, the pure noise series produces a slowing decreasing sequence of singular values. The explicit plateau in the spectra represents the ordinal numbers of paired eigen triples. The eigen triples 2–3 for the sunspot data corresponds to 11 years period; eigen triples for 1–2, 3–5, 6–10, 11–14 for the WH temperature data are related to harmonic with specific periods (periods 33–35, 11, 5, 2); eigen triples for 2–5, 6–9, 10–13 for the geomagnetic data are related to periods 11, 5, 2 years. The eigen triples for the SOI data represents to ~ 5–7, 2 years periods. In order to assess periodicities, the periodogram and the wavelet power spectra are plotted to the SSA reconstructed data (SSA-RC) (Fig. 7). From the Fig. 7, the periodogram of SSA-RC of SSN and Geomagnetic data shows strong power at ~ 120, 10–11 years; the SOI data shows strong peaks at 6–9, 3 years and WH data shows strong power at ~ 32, ~ 10–11, 3–5 years. The wavelet spectra for all the SSA-RC data confirms the results excepts for periods at ~ 120 years as the scaling period for the wavelet spectra is 64 years period. The coherency plot of the SSA-RC data sets (Fig. 8) indicates a significant power at 33, 11 years, 2–7 years in the WH temperature record suggesting the possible influences of sunspot–geomagnetic activity and ENSO through tele-connection and hence significant role of these remote internal oscillations of the atmosphere–ocean system on the Indian monsoon system. Researchers have attributed these phenomena to internal ocean dynamics and involve ocean atmospheric coupling as well as variability in the strength of thermohaline circulations (Knight et al., 2005; Delworth and Mann, 2000).

In general our result agrees well with earlier findings in sense that statistically significant global cycles of coupled effects of sunspot/geomagnetic and ENSO are present in the land based temperature variability record. However, there are certain striking features in the spectra that need to be emphasized regarding the western Himalayas temperature variability: (i) interannual cycles in period range of 3–8 years corresponding to ENSO in the wavelet spectra exhibit intermittent oscillatory characteristics throughout the large portion of the record (Fig. 4); (ii) the 11 years solar cycle in the cross wavelet spectrum of SSN and SOI (Fig. 5) indicate the solar modulation in the ENSO

NPGD
2, 1447–1479, 2015

phenomena. (iii) The high amplitude at 11 years in the time intervals 1900–1995 with a strong intensity from 1900–1995 shows a good correspondence with the high temperature variability for the interval of high solar–geomagnetic activity. The Multi-decadal (30–40 years) periodicity identified here in Western Himalayan tree ring temperature record matches with North Atlantic sea surface temperature variability implying that the temperature variability in the western Himalayan is not a regional phenomenon, but a globally teleconnected climate phenomena associated with the global ocean–atmospheric dynamics system (Tiwari and Sri Lakshmi, 2009; Delworth et al., 1993; Stocker, 1994). The coupled ocean–atmosphere system appears to transport energy from the hot equatorial regions towards Himalayan territory in a cyclic manner. These results may provide constraints for modeling of climatic variability over the Indian region and ENSO phenomena associated with the redistribution of temperature variability. The solar–geomagnetic effects plays a major role in abnormal heating the land surface thereby indirectly affect the atmospheric temperature gradient between the land–ocean coupled system. In the present work, the connections between solar–geomagnetic activity and ENSO on the WH time series are found to be statistically highly significant, especially when they are studied over contrasting epochs of respectively high and low solar activity. The correlation plots for the SSA-RC data sets of WH–sunspot, WH–aa Index, WH–SOI and sunspot–aa Index are plotted in Fig. 9. It is noticed that there is a correlation plots for the geomagnetic–sunspot activity has a maximum correlation value at 1 year lag suggesting the strong influence of sunspot and geomagnetic forcing on one another. The cross-correlation plot for the WH data and the SOI represents a maximum value at zero lag. The correlations plot for WH–sunspot and WH–geomagnetic index exhibits almost the same results suggesting the possible impact of solar flares on the Indian temperature variability.

The net effect of solar activity on temperature record therefore appears to be the result of cooperating or counteracting influences on the short and long periods, depending on the indices used; scale-interactions therefore appear to be important. Nev-

NPGD
2, 1447–1479, 2015

ertheless, the link between Indian climate and solar–geomagnetic activity emerges as having the strongest evidence; next is the ENSO–solar activity connection.

5 Conclusions

We have presented here a new spectral approach to identify the periodic patterns from the published Indian temperature variability records. This study of SSA-wavelet spectral methods and the wavelet analysis of the SSA reconstructed time series highlights the removal of noise in the data and identifies the existence of a high-amplitude, recurrent, multidecadal scale patterns present in Indian temperature records. The Wavelet spectral analysis of SSA reconstructed data identifies significant peaks around 33, 11, 2–7 years (95 % confidence) in the WH temperature record. The coherency plots of the SSA reconstructed WH–sunspot; WH–geomagnetic and WH–SOI data sets shows strong spectral signatures in the whole record confirming the possible influences of sunspot–geomagnetic activity and ENSO through tele-connection and hence the significant role of these remote internal oscillations of the atmosphere–ocean system on the Indian temperatures. We conclude that the signature of solar–geomagnetic activity affects exists on the surface air temperatures of Indian continent. However, long data sets from the different sites on the Indian continent are necessary to identify the influences of the 120 years solar–geomagnetic cycles.

Acknowledgements. We thank R. R. Yadav for kindly providing his data. We are thankful to A. Grinsted and his colleagues for providing the wavelet software package. We are very grateful to the Head, UCESS, University of Hyderabad for his support and kind permission to publish this paper.

NPGD
2, 1447–1479, 2015

References

Appenzeller, C., Stocker, T. F., and Anklin, M.: North Atlantic Oscillation dynamics record in Greenland ice cores, Science, 282, 446–449, 1998.

Barnett, T. P., Dumenil, L., Schlese, U., Roeckner, E., and Latif, M.: The effect of Eurasian snow cover on regional and global climate variations, J. Atmos. Sci., 48, 661–685, 1989.

Benestad, R. E. and Schmidt, G. A.: Solar trends and global warming, J. Geophys. Res., 114, D14101, doi:10.1029/2008JD011639, 2009.

Bhattacharyya, A. and Chaudhary, V.: Late-summer temperature reconstruction of the eastern Himalayan region based on tree-ring data of Abies densa, Arct. Antarct. Alp. Res., 35, 196–202, 2003.

Bhattacharyya, A. and Yadav, R. R.: Tree growth and recent climatic changes in the western Himalaya, Geophytology, 22, 255–260, 1992.

Bhattacharyya, A. and Yadav, R. R.: Dendrochronological reconnaissance of *Pinus wallichiana* to study glacial behaviour in the western Himalaya, Current Sci., 70, 739–744, 1996.

Bhatacharyya, A., LaMarche, V. C., and Telewski, F. W.: Dendrochronological reconnaissance of the conifers of Northwest India, Tree-Ring Bull., 48, 21–30, 1988.

Bhattacharyya, A., Yadav, R. R., Borgaonkar, H. P., and Pant, G. B.: Growth ring analysis of Indian tropical trees: dendroclimatic potential, Current Sci., 62, 736–741, 1992.

Bhattacharyya, A., Shah, S. K., and Chaudhary, V.: Would tree-ring data of *Betula utilis* be potential for the analysis of Himalayan Glacial fluctuations?, Current Sci., 91, 754–761, 2006.

Bigg, G. R.: The Oceans and Climate, Cambridge University Press, Cambridge, 1–266, 1996.

Borgaonkar, H. P., Pant, G. B., and Rupa Kumar, K.: Ring width variations in *Cedrus deodara* and its climatic response over the western Himalaya, Int. J. Climatol., 16, 1409–1422, 1996.

Broomhead, D. S. and King, G. P.: Extracting qualitative dynamics from experimental data, Physica D, 20, 217–236, 1986.

Budyko, M. I.: The effect of solar radiation variations on the climate of the Earth, Tellus, 21, 611–619, 1969.

Cane, M. A.: Tropical Pacific ENSO models: ENSO as a mode of the coupled system, in: Climate System Modelling, edited by: Trenberth, K. E., Cambridge University Press, Cambridge, 583–614, 1992.

Chaudhary, V., Bhattacharyya, A., and Yadav, R. R.: Tree-ring studies in the eastern Himalayan region: prospects and problems, IAWA J., 20, 317–324, 1999.

NPGD

2, 1447–1479, 2015

Study of the imprints of Solar–ENSO–Geomagnetic activity on Indian climate

S. Sri Lakshmi and R. K. Tiwari

Chowdary, J. S., Gnanseelan, C., Vaid, B. H., and Salvekar, P. S.: Changing trends in the tropical Indian Ocean SST during La Nina years, Geophys. Res. Lett., 33, L18610, doi:10.1029/2006GL026707, 2006.

Chowdary, J. S., John, N., and Gnanseelan, C.: Interannual variability of surface air–temperature over India: impact of ENSO and Indian Ocean Sea surface temperature, Int. J. Climatol., 34, 416–429, 2014.

Cole, J. E., Fairbanks, R. G., and Shen, G. T.: Recent variability in the Southern Oscillation: isotopic results from a Tarawa Atoll coral, Science, 260, 1790–1793, 1993.

De Freitas, C. and Mclean, J.: Update of the chronology of natural signals in the near-surface mean global temperature record and the Southern Oscillation Index, Int. J. Geosci., 4, 234–239, 2013.

Delworth, T. and Mann, M.: Observed and stimulated multideacadl variability in the Northern Hemisphere, Clim. Dynam., 16, 661–676, 2000.

Delworth, T., Manabe, S., and Stouffer, R. J.: Interdecadal variations of the thermohaline circulation in a coupled ocean–atmosphere model, J. Climate, 6, 1991–2011, 1993.

El-Borie, M. A. and Al-Thoyaib, S. S.: Can we use the aa geomagnetic activity index to predict partially the variability in global mean temperature, J. Phys. Sci., 1, 67–74, 2006.

El-Borie, M. A., Al Thoyaib, S. S., and Al-Sayed, N.: The possible rule of solar activity in variability of global mean temperature temperature, in: The 2nd Inter Conf. of Physics and Material Science, 1, 302 pp., 2007.

El-Borie, M. A., Shafik, E., Abdel-Halim, A. A., and El-Monier, S.: Spectral analysis of solar variability and their possible role on the global warming (1880–2008), J. Environ. Protect., 1, 111–120, 2010.

Feng, S. H., Kaufman, D., Yoneji, S., Nelson, D., Shemesh, A., Huang, Y., Tian, J., Bond, G., Benjamin, C., and Brown, T.: Cyclic variation and solar forcing of Holocene climate in the Alaskan Subarctic, Science, 301, 1890–1893, 2003.

Foufoula-Georgiou, E. and Kumar, P. (Eds.): Wavelets in Geophysics, Academic, San Diego, Calif., 373 pp., 1995.

Friis, C. E. and Lassen, K.: Length of the solar cycle: an indicator of solar activity closely associated with climate, Science, 254, 698–700, 1991.

Friis, C. E. and Svensmark, H.: What do we really know about the sun–climate connection?, Adv. Space Res., 20, 913–9211, 1997.

NPGD

2, 1447–1479, 2015

Study of the imprints of Solar–ENSO–Geomagnetic activity on Indian climate

S. Sri Lakshmi and R. K. Tiwari

Frohlich, C. and Lean, J.: solar radiative output and its variability: evidence and mechanisms, Astron. Astrophys. Rev., 12, 273–320, 2004.
Gray, S. T., Graumlich, L. J., Betancourt, J. L., and Pederson, G. T.: A tree-ring based reconstruction of the Atlantic Multidecadal Oscillation since 1567 A.D., Geophys. Res. Lett., 31, L12205, doi:10.1029/2004GL019932, 2004.
Gray, W. M., Sheaffer, J. D., and Knaff, J. A.: Hypothesized mechanism for stratospheric QBO influence on ENSO variability, Geophys. Res. Lett., 19, 107–110, 1992.
Grinsted, A., Moore, J. C., and Jevrejeva, S.: Application of the cross wavelet transform and wavelet coherence to geophysical time series, Nonlin. Processes Geophys., 11, 561–566, doi:10.5194/npg-11-561-2004, 2004.
Gu, D. and Philander, S. G. H.: Secular changes of annual and inter-annual variability in the tropics during the past century, J. Climate, 8, 64–876, 1995.
Holschneider, M.: Wavelets: an Analysis Tool, Oxford University Press, New York, 455 pp., 1995.
Horel, J. D. and Wallance, J. M.: Planetary-scale atmospheric phenomena associated with the Southern Oscillation, Mon. Weather Rev., 109, 813–829, 1981.
Hughes, M. K.: Dendroclimatic evidence from the western Himalaya, in: Climate Since AD 1500, edited by: Bradlay, R. S. and Jones, D., Routledge, London, 415–431, 1992.
Jevrejeva, S., Moore, J. C., and Grinsted, A.: Influence of the Arctic Oscillation and El Niño–Southern Oscillation (ENSO) on ice conditions in the Baltic Sea: the wavelet approach, J. Geophys. Res., 108, 4677, doi:10.1029/2003JD003417, 2003.
Ji, J. F., Shen, J., Balsam, W., Chen, J., Liu, L., and Liu, X. Q.: Asian monsoon oscillations in the northeastern Qinghai–Tibet Plateau since the late glacial as interpreted from visible reflectance of Qinghai Lake sediments, Earth Planet. Sc. Lett., 233, 61–70, 2005.
Kasatkina, E. A., Shumilov, O. I., and Krapiec, M.: On periodicities in long term climatic variations near 68° N, 30° E, Adv. Geosci., 13, 25–29, doi:10.5194/adgeo-13-25-2007, 2007.
Kiladis, G. N. and Diaz, F. H.: Global climatic anomalies associated with extremes in the Southern Oscillation, J. Climate, 2, 1069–1090, 1989.
Knight, J. R., Allan, R. J., Folland, C. K., Vellinga, M., and Mann, M. E.: A signature of persistent natural thermohaline circulation cycles in observed climate, Geophys. Res. Lett., 32, L20708, doi:10.1029/2005GL024233, 2005.

Kothwale, D. R., Munot, A. A., and Krishna Kumar, K.: Surface air temperature variability over India during 1901–2007 and its association with ENSO, Clim. Res., 42, 89–104, doi:10.3354/cr00857, 2010.
Labitzke, K. and Van Loon, H.: Association between the 11-year cycle, the QBO and the atmosphere, J. Climate, 2, 554–565, 1989.
Labitzke, K. and Van Loon, H.: Association between the 11-year solar cycle and the atmosphere, Part V: Summer, J. Climate, 5, 240–251, 1992.
Labitzke, K. and Van Loon, H.: Some recent studies of probable connections between solar and atmospheric variability, Ann. Geophys., 11, 1084–1094, 1993, http://www.ann-geophys.net/11/1084/1993/.
Lean, J., Beer, J., and Bradley, R.: Reconstruction of solar irradiance since 1610: implications for climate change, Geophys. Res. Lett., 22, 3195–3198, 1995.
Lean, J. L. and Rind, D. H.: How natural and anthropogenic influences alter global and regional surface temperatures: 1889 to 2006, J. Geophys. Res. Lett., 35, L18701, doi:10.1029/2008GL034864, 2008.
Mann, M. E., Park, J., and Bradley, R. S.: Global interdecdal and century-scale climate oscillations during the past 5 centuries, Nature, 378, 266–27, 1995.
Meehl, G. A., Arblaster, J. M., Matthes, K., Sassi, F., and Van Loon, H.: Amplifying the Pacific climate system response to a small 11-year solar cycle forcing, Science, 325, 1114–1118, 2009.
Mendoza, B., Perez-Enriquez, R., and Alvarez-Madrigal, M.: Analysis of solar activity conditions during periods of El Niño events, Ann. Geophys., 9, 50–54, 1991, http://www.ann-geophys.net/9/50/1991/.
Mokhov, I. I., Eliseev, A. V., Handorf, D., Petukhov, V. K., Dethloff, K., Weishiemer, A., and Khvorostyanov, D. V.: North Atlantic Oscillation: diagnosis and simulation of decadal variability and its long period evolution, Atmos. Ocean Phys., 36, 555–565, 2000.
Nicolson, S. E.: An analysis of the ENSO signal in the tropical Atlantic and Western Indian oceans, Int. J. Climatol., 17, 345–375, 1997.
Pant, G. B. and Rupa Kumar, K.: Climates of South Asia, John Wiley and Sons, Chichester, 320 pp., 1997.
Philander, S. G.: El Niño, La Nina and the Southern Oscillation, Academic Press, London, 1–293, 1990.

Proctor, C. J., Baker, A., and Barnes, W. L.: A three thousand year record of North Atlantic climate, Clim. Dynam., 19, 449–454, 2002.
Reid, G. C.: Solar irradiance variations and global ocean temperature, J. Geomagn. Geoelectr., 43, 795–801, 1991.
Reid, G. C. and Gage, K. S.: The climatic impact of secular variations in solar irradiance, in: Secular Solar and Geomagnetic Variations in the Last 10 000 Years, NATO AS Series, edited by: Stephenson, F. R. and Wolfendale, A. W., Kluwer, Dordrecht, 225–243, 1988.
Rigozo, N. R., Noredmann, D. J. R., Echer, E., Zanandrea, A., and Gonzalez, W. D.: Solar variability effects studied by tree-ring data wavelet analysis, Adv. Space Res., 29, 1985–1988, 2002.
Rigozo, N. R., Vieira, L. E. A., Echer, E., and Nordemann, D. J. R.: Wavelet analysis of Solar–ENSO imprints in tree-ring data from southern Brazil in the last century, Climatic Change, 60, 329–340, 2003.
Rigozo, N. R., Nordeman, D. J. R., Echer, E., Vieira, L. E. A., Echer, M. P. S., and Prestes, A.: Tree-ring width wavelet and spectral analysis of solar variability and climatic effects on a Chilean cypress during the last two and a half millennia, Clim. Past Discuss., 1, 121–135, doi:10.5194/cpd-1-121-2005, 2005.
Rigozo, N. R., Nordeman, D. J. R., Silva, H. E., Echer, M. P. S., and Echer, E.: Solar and climate signal records in tree ring width from Chile (AD 1587–1994), Planet. Space Sci., 55, 158–164, 2007.
Shah Santosh, K., Bhattacharyya, A., and Chaudhary, V.: Reconstruction of June–September precipitation based on tree-ring data of Teak (*Tectona grandis* L.) from Hoshangabad, Madhya Pradesh, India, Dendrochronologia, 25, 57–64, 2007.
Steinhilber, F., Beer, J., and Frohlich, C.: Total solar irradiance during the Holocene, Geophys. Res. Lett., 36, L19704, doi:10.1029/2009GL040142, 2009.
Stocker, T. F.: The variable ocean, Nature, 367, 221–222, 1994.
Tiwari, R. K. and Srilakshmi, S.: Periodicities and non-stationary modes in tree ring temperature variability record of the Western Himlayas by multitaper and wavelet spectral analyses, Current Sci., 97, 705–709, 2009.
Torrence, C. and Compo, G. P.: A practical guide to wavelet analysis, B. Am. Meteorol. Soc., 79, 61–78, 1998.
Torrence, C. and Webster, P.: Interdecadal changes in the ESNO–monsoon system, J. Climate, 12, 2679–2690, 1999.

NPGD
2, 1447–1479, 2015

Trenberth, K. and Hoar, T. J.: El Niño and climate change, Geophys. Res. Lett., 24, 3057–3060, 1997.
Tsonis, A. A., Elsner, J. B., Hunt, A. G., and Jagger, T. H.: Unfolding the relation between global temperature and ENSO, Geophys. Res. Lett., 32, L09701, doi:10.1029/2005GL022875, 2005.
Vautard, R. and Ghil, M.: Singular spectrum analysis in nonlinear dynamics, with applications to paleoclimatic time series, Physica D, 35, 395–424, doi:10.1016/0167-2789(89)90077-8, 1989.
Weng, H. and Lau, K.-M.: Wavelets, period doubling, and time-frequency localization with application to organizationmof convection over the tropical western Pacific, J. Atmos. Sci., 51, 2523–2541, 1994.
Wiles, G. C., D'Arrigo, R. D., and Jacoby, G. C.: Gulf of Alaska atmosphere–ocean variability over recent centuries inferred from coastal tree-ring records, Climatic Change, 38, 289–306, 1998.
Yadav, R. R., Park, W. K., and Bhattacharyya, A.: Spring-temperature variations in western Himalaya, India, as reconstructed from tree-rings: AD 1390–1987, Holocene, 9, 85–90, 1999.
Yadav, R. R., Park, W. K., Singh, J., and Dubey, B.: Do the western Himalayas defy global warming?, Geophys. Res. Lett., 31, L17201, doi:10.1029/2004GL020201, 2004.
Yasunari, T.: Zonally propagating modes of the global east-west circulation associated with the Southern Oscillation, J. Meteorol. Soc. Jpn., 63, 1013–1029, 1985.

NPGD
2, 1447–1479, 2015

Study of the imprints of Solar–ENSO–Geomagnetic activity on Indian climate

S. Sri Lakshmi and R. K. Tiwari

Title Page
Abstract | Introduction
Conclusions | References
Tables | Figures
◀| |▶
◀ ▶
Back | Close
Full Screen / Esc
Printer-friendly Version
Interactive Discussion

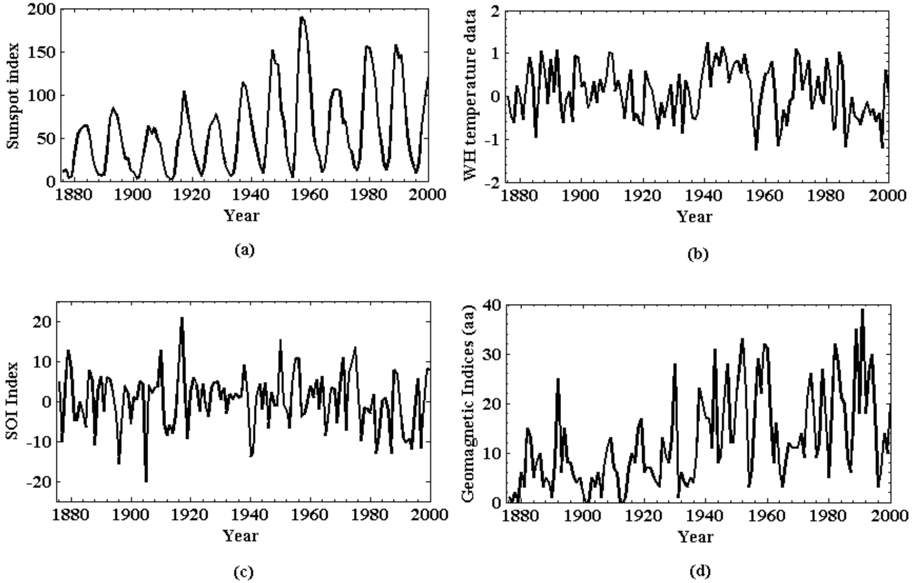

Figure 1. Time series of **(a)** Sunspot Index, **(b)** the mean pre-monsoon temperature anomalies of the western Himalayas, **(c)** SOI index and **(d)** geomagnetic indices (aa Index) for common period 1876–2000.

NPGD
2, 1447–1479, 2015

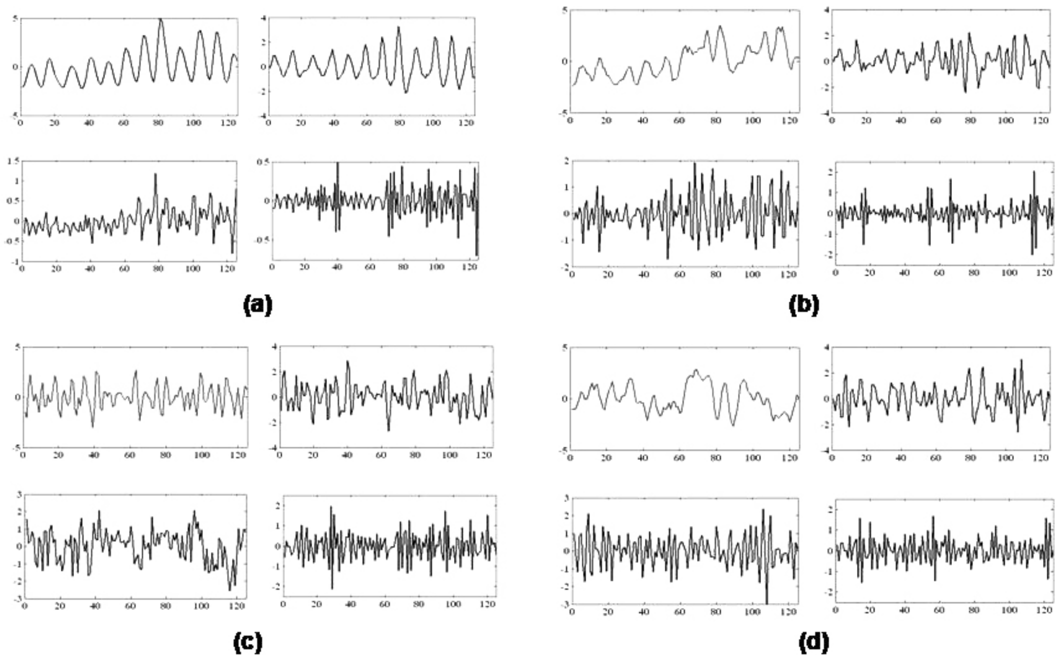

Figure 2. Principal components (PC1, PC2, PC3 and PC4) for **(a)** Sunspot Index, **(b)** geomagnetic indices (aa Index), **(c)** SOI index and **(d)** the mean pre-monsoon temperature anomalies of the western Himalayas for common period 1876–2000 (125 data points).

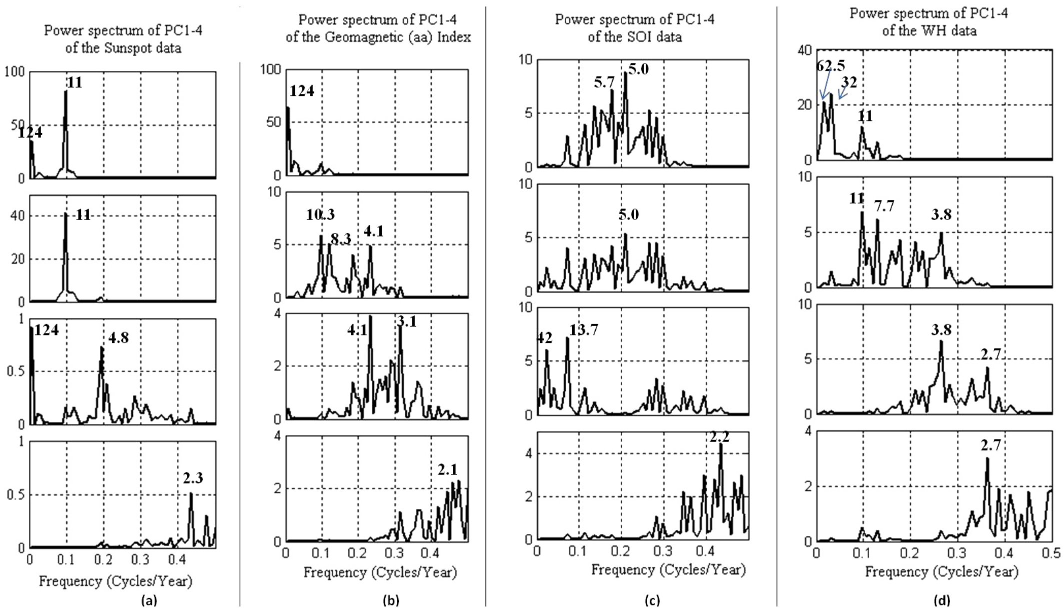

Figure 3. Power spectra of the principal component (PCs) (PC1–4 shown in Fig. 3) for all the data sets with their significant periodicities indicated in bold letters.

NPGD

2, 1447–1479, 2015

Study of the imprints of Solar–ENSO–Geomagnetic activity on Indian climate

S. Sri Lakshmi and R. K. Tiwari

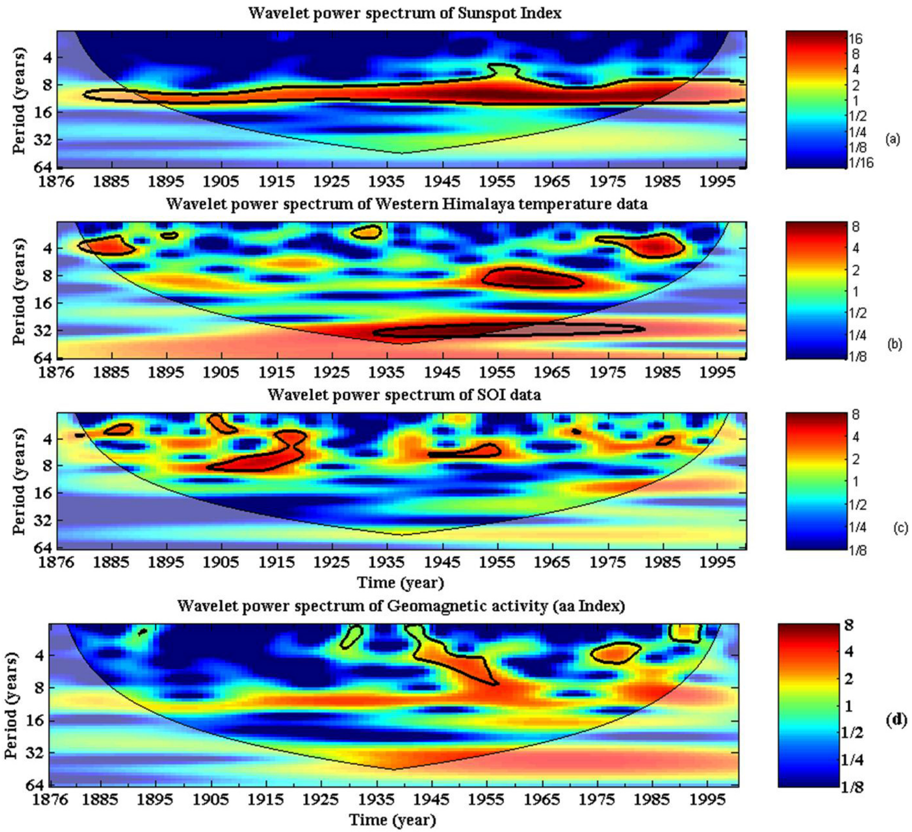

Figure 4. Wavelet power spectrum of **(a)** sunspot number, **(b)** western Himalaya temperature data, **(c)** SOI and **(d)** geomagnetic activity (aa indices) with cone of influence (lighter shade smooth curve) and black lines indicate significant power on 95 % level compared to red noise based on AR(1) coefficient. The legend on right indicates the cross-wavelet power.

NPGD
2, 1447–1479, 2015

S. Sri Lakshmi and R. K. Tiwari

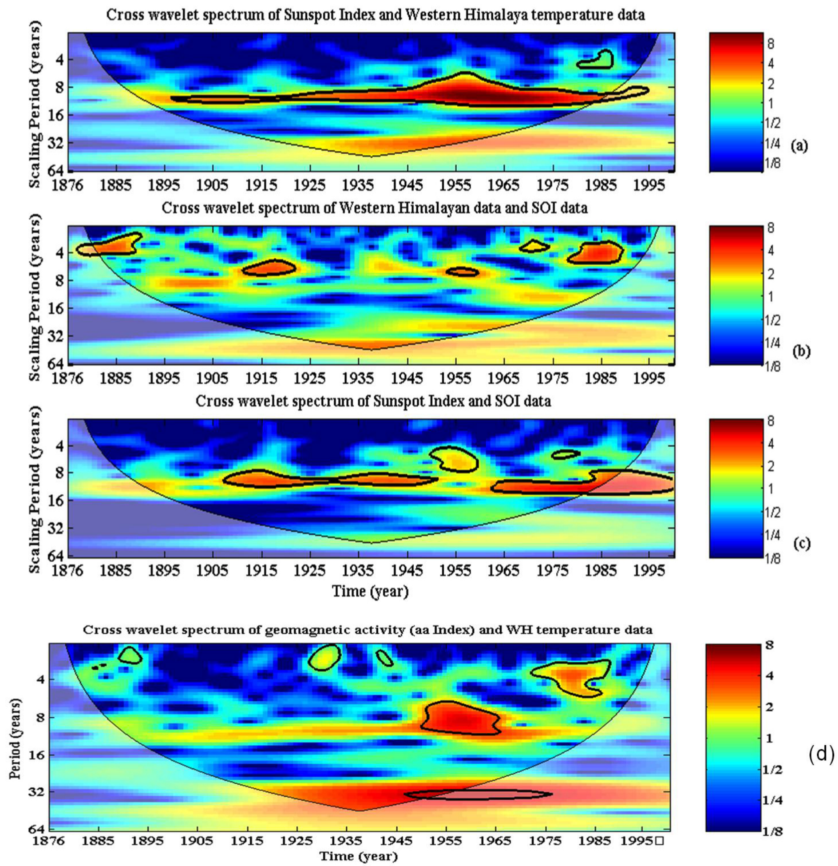

Figure 5. Cross wavelet spectrum between **(a)** WH–SSN, **(b)** WH–SOI, **(c)** SSN–SOI and **(d)** geomagnetic activity and WH with cone of influence (lighter shade smooth curve) and black lines indicate significant power on 95 % level compared to red noise based on AR(1) coefficient. The legend on right indicates the cross-wavelet power.

NPGD
2, 1447–1479, 2015

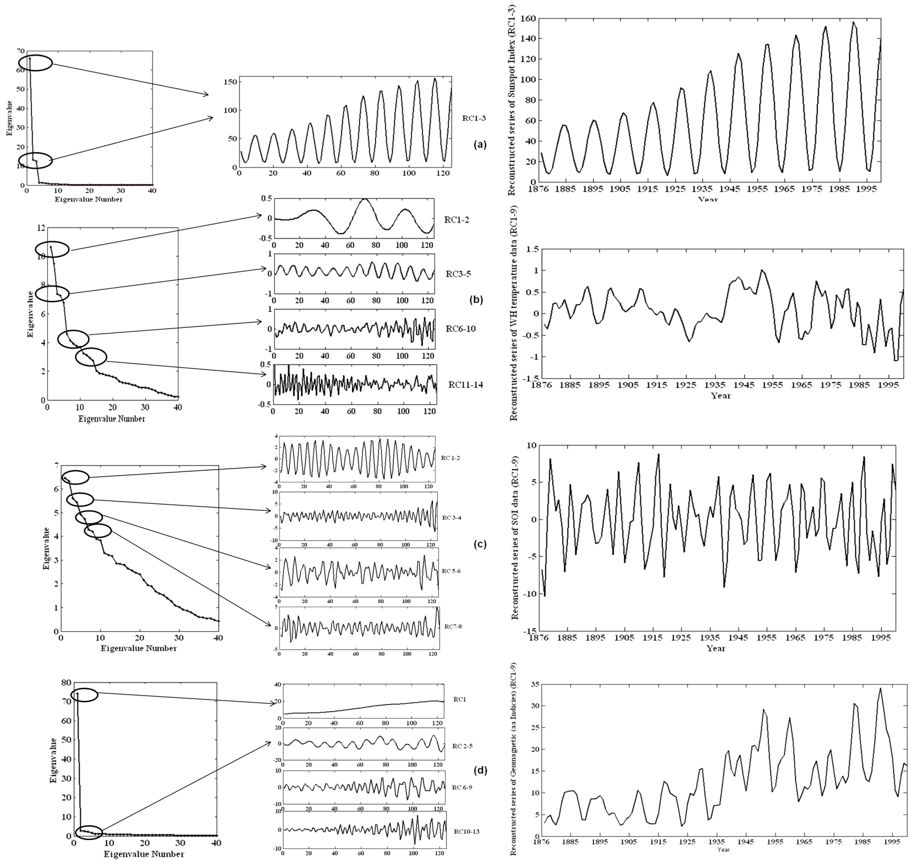

Figure 6. Singular spectra with its SSA decomposed components and its reconstructed time series for **(a)** sunspot number, **(b)** western Himalaya temperature data, **(c)** SOI and **(d)** geomagnetic activity (aa indices).

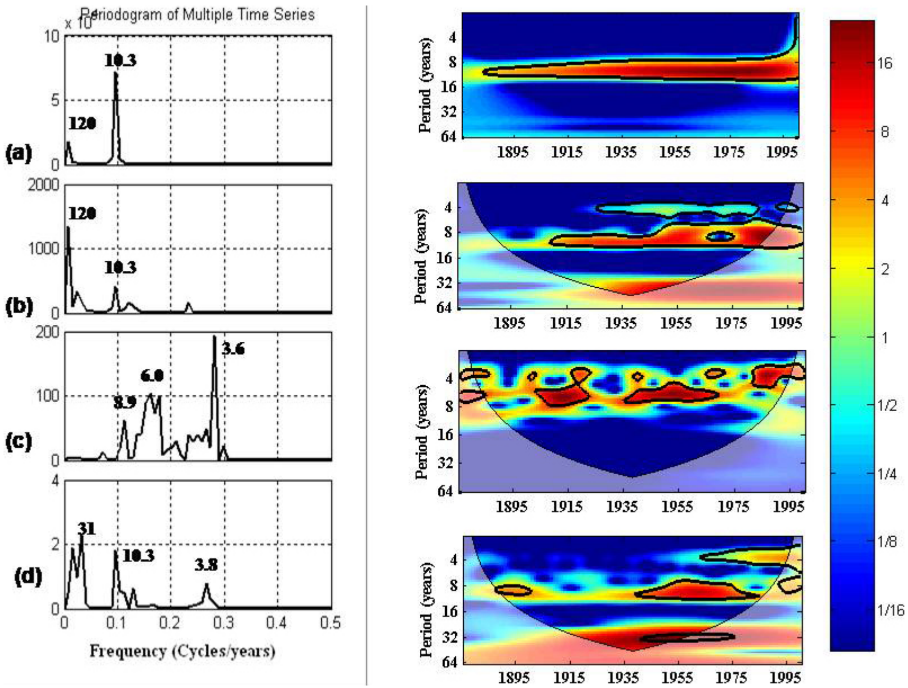

Figure 7. Power spectrum and wavelet power spectrum of SSA reconstructed **(a)** sunspot data, **(b)** geomagnetic indices (aa Index), **(c)** SOI index and **(d)** the western Himalayas temperature data with cone of influence (lighter shade smooth curve) and black lines indicate significant power on 95 % level compared to red noise based on AR(1) coefficient. The legend on right indicates the cross-wavelet power.

NPGD
2, 1447–1479, 2015

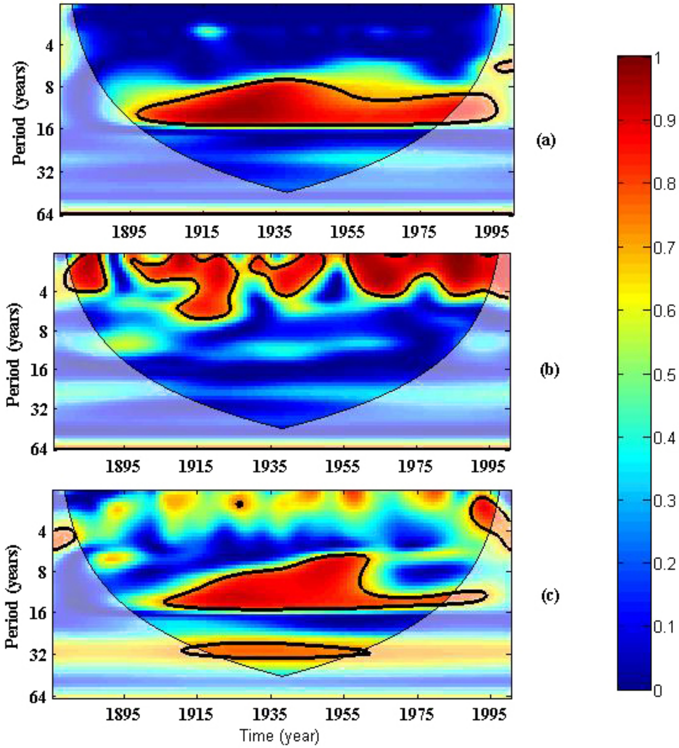

Figure 8. Squared wavelet coherence plotted for the SSA reconstructed time series between **(a)** WH–SSN, **(b)** WH–SOI and **(c)** WH–aa Index with cone of influence (lighter shade smooth curve) and black lines indicate significant power on 95 % level compared to red noise based on AR(1) coefficient.

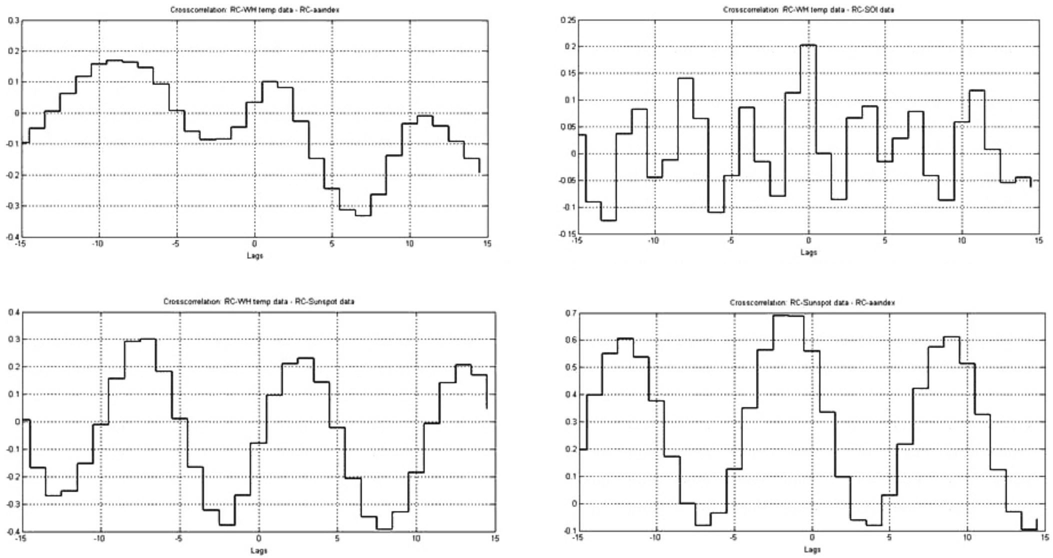

Figure 9. Cross-correlation of SSA reconstructed time series of WH–aa Index; WH–SOI; WH–SSA and SSN–aa Index.

NPGD

2, 1447–1479, 2015

Study of the imprints of Solar–ENSO–Geomagnetic activity on Indian climate

S. Sri Lakshmi and R. K. Tiwari